LAWRENCE
LIVERMORE
NATIONAL
LABORATORY

LLNL-JRNL-584232

Binding of apolipoprotein E inhibits the oligomer growth of amyloid beta in solution as determined by fluorescence cross correlation spectroscopy

S. Ly, R. Altman, J. Petrlova, Y. Lin, T. Huser, T. A. Laurence, J. C. Voss

September 24, 2012

Journal of Biological Chemistry

Disclaimer

Binding of apolipoprotein E inhibits the oligomer growth of amyloid beta in solution as determined by fluorescence cross correlation spectroscopy*

Sonny Ly[a,c,1], Robin Altman[b,1], Jitka Petrlova[b], Yu Lin[c], Thomas Huser[c], Ted A. Laurence[a], and John C. Voss[b]

[a] Physical and Life Science Directorate, Lawrence Livermore National Laboratory, Livermore, CA 94550
[b] Department of Biochemistry and Molecular Medicine, University of California, Davis, Davis, CA 95616
[c] NSF Center for Biophotonics Science and Technology, University of California, Davis, Sacramento, CA 95817

*****Running title: *Binding of apolipoprotein E to amyloid beta*

[1] Author contributions: S. Ly and R. Altman contributed equally to this work.

To whom correspondence should be addressed: Dept. of Biochemistry & Molecular Medicine, 4303 Tupper Hall, Davis ,CA 95616 Tel: (530)754-7583 Email: jcvoss@ucdavis.edu

ABSTRACT

Background: ApoE is the most significant risk factor for Alzheimer's disease and affects the processing of Aβ in the brain.
Results: ApoE binds to aggregating Aβ peptides and maintains a faster diffusion rate for the Aβ peptide over time.
Conclusion: Binding of apoE to Aβ slows the oligomerization of Aβ.
Significance: This may help explain a central mechanism for Aβ balance in the brain.

ABSTRACT

One of the primary neuropathological hallmarks of Alzheimer's disease is the presence of extracellular amyloid plaques resulting from the aggregation of amyloid beta (Aβ) peptides. The intrinsic disorder of the Aβ peptide drives self-association and progressive re-ordering of the conformation in solution, and this dynamic distribution of Aβ complicates biophysical studies. This property poses a challenge for understanding the interaction of Aβ with apolipoprotein E (apoE). ApoE plays a pivotal role in the aggregation and clearance of Aβ peptides in the brain, and the ε4 allele of APOE is the most significant known genetic modulator of Alzheimer's risk. Understanding the interaction between apoE and Aβ will provide insight into the mechanism by which different apoE isoforms determine Alzheimer's disease risk. Here we applied alternating laser excitation fluorescence cross correlation spectroscopy to observe the single molecule interaction of Aβ with apoE in the hydrated state. The diffusion time of freely diffusing Aβ in the absence of apoE shows significant self-aggregation, whereas in the presence of apoE, binding of the protein results in a more stable complex. These results show that apoE slows down the oligomerization of Aβ in solution, and provide direct insight into the process by which apoE influences the deposition and clearance of Aβ peptides in the brain. Furthermore, by developing an approach to remove signals arising from very large Aβ aggregates, we show that real-time single particle observations provide access to information regarding the fraction of apoE bound and the stoichiometry of apoE and Aβ in the complex.

INTRODUCTION

Alzheimer's disease (AD) is a neurodegenerative disorder of aging that affects the cognitive ability of the brain. AD is characterized by two histopathological features of the brain: insoluble extracellular plaques comprised of amyloid beta (Aβ) peptides, and intracellular neurofibrillary tangles formed from hyperphosphorylated *tau*, a microtubule-associated protein. Although the primary cause and progression of AD are still not well understood, they are thought to be linked to the aggregation of Aβ peptides. The Aβ peptides are generated as cleavage fragments by the action of γ and β secretases on the amyloid precursor protein, a constitutively expressed transmembrane

protein. Due to their inherently disordered and "sticky" nature, the resulting Aβ peptides easily aggregate into oligomers, then fibrils, and finally, mature plaques in the brain.

To date, the ε4 allele of the apolipoprotein E (APOE) gene is the strongest known risk factor for the late-onset form of AD [1-3]. The apoE protein is involved in lipid transport throughout the body, and is the principal lipid transport protein in the central nervous system. There are three apoE isoforms: E2, E3, and E4, and studies have demonstrated increased risk of AD and earlier age of onset in individuals carrying the ε4 allele. While the ε4 allele is linked to both sporadic and familial late-onset forms of AD, the mechanism of this association remains unknown. However, studies have revealed the presence of apoE in the amyloid fibrils and plaques of Alzheimer's brains, which strongly suggests that apoE plays a critical role in the pathogenesis of AD through its interaction with aggregating Aβ peptides [4-6]. It has also been established that apoE plays an important role in the homeostasis of Aβ in the brain, through its influence on both the deposition and clearance of the peptide [7-11]. However, the interaction of Aβ with apoE is still poorly understood, with conflicting evidence with respect to differences in isoform interaction with Aβ[9]. In addition, many previous studies were also designed with particular attention on isoform influence on amyloid burden rather than Aβ toxicity, and therefore focused on apoE associations with fibril/plaque species rather than the oligomeric forms of Aβ that are now recognized as the pathogenic species. As oligomeric Aβ represents a dynamic interrmediate along the fibrilization pathway, it is very difficult to investigate this interaction and determine the affinity of apoE with Aβ directly in solution, particularly at the single molecule level. We therefore require insights into the oligomeric state of Aβ, its binding with apoE, and the distribution of these species across the system to understand how apoE influences Aβ deposition and clearance in the brain.

Fluorescence correlation spectroscopy (FCS) is a statistical technique to detect chemical reactions and determine translational and rotational diffusion coefficients of molecules and complexes [12-14]. It is based on monitoring intensity fluctuations emitted from fluorescent molecules diffusing through a tightly focused laser excitation volume (~1 femtoliter). By subjecting these fluctuations to an autocorrelation analysis, $G^{(2)}(\tau) = \frac{\langle I(t)I(t+\tau)\rangle}{\langle I\rangle^2}$, the molecular diffusion time, sample concentration, and photophysical properties can be extracted. With precise knowledge of the diffusion time, τ_D, and beam waist, ω, of the excitation laser spot, the diffusion coefficient, $D = \frac{\omega^2}{4\tau_D}$ can be determined which is proportional to the Einstein-Stokes hydrodynamic radius $R_H = \frac{K_B T}{6\pi n_0 D}$.

If two differently labeled species are in the sample, their colocalization can be monitored using fluorescence cross correlation spectroscopy (FCCS), originally developed by Schwille [15]. FCCS has been applied to study binding events [16], enzyme kinetics such as oligonucleotide cleavage [17] and protease cleavage [18], and to monitor calcium activity in cells containing calmodulin [19]. The addition of alternating laser excitation (ALEX) eliminates spectral cross-talk between fluorophores and reduces the possibility of false positives, because the different fluorophores are not excited simultaneously and their signals can be temporally separated. ALEX was first developed by Kapanidis et al. for fluorescence resonance energy transfer (FRET) measurements to determine the stoichiometry between biomolecules It was first developed by Kapanidis for fluorescence resonance energy transfer (FRET) measurements [20], and later extended to FCCS to eliminate cross-talk between two fluorescent proteins in cells [21], to monitor single molecule interactions [22, 23], and also to antibody-based protein detection [24].

We apply ALEX-FCCS to investigate the interaction of apoE3 with Aβ in the hydrated state. The ability of this technique to report on the distribution of Aβ species, along with the binding of Aβ to other proteins, provides a powerful tool for studying the peptide's interaction with apoE in the oligomeric state. To probe the molecular basis of apoE's role in the development of Alzheimer's disease, the E3 isoform was selected as a representative example for this study. Because the

fluorescent labeling required for this study takes advantage of thiol binding chemistry at a cysteine residue, it was necessary to avoid binding to the native cysteine residue found at position 112 in apoE3. Thus, we utilized the apoE3-like (apoE3L) protein, in which a serine is substituted for the cysteine at position 112. A thiol-reactive fluorescent label was then introduced to the C-terminal domain of apoE3L by replacing Trp264 with a cysteine residue. It has been shown that the cysteine substitution and subsequent modification of the W264C mutation of apoE3L with the thiol-specific label does not alter its predicted distribution among plasma lipoproteins, and circular dichroism analysis of the labeled protein is indistinguishable from the wild-type apoE [25].

EXPERIMENTAL PROCEDURES

Materials

Hexafluoro-2-propanol (HFIP) was purchased from Sigma-Aldrich (St. Louis, MO). Dimethyl sulfoxide (DMSO) was purchased from Fisher Scientific (Pittsburgh, PA). Alexa Fluor 488 C_5-maleimide was obtained from Invitrogen Molecular Probes (Carlsbad, CA) and Atto 647N NHS ester was obtained from Fluka Analytical, Sigma-Aldrich (St. Louis, MO).

Preparation of Amyloid β

Amyloid-$\beta_{(1-40)}$ peptide was purchased from Bachem (catalog number H-1194, Torrance, CA). The peptide was dissolved in HFIP and incubated at room temperature with gentle rocking for 48-72 hours. SpeedVac or evaporation was then used to remove the HFIP, resulting in a monomeric Aβ pellet. To direct preferential labeling of the N-terminal amine group of Aβ, a 0.1 mg aliquot of peptide was dissolved in 10 μL DMSO and reacted at pH 7.0 with 3 μL Atto 647N NHS ester label (10 mM stock in DMSO) and 500 μL phosphate-buffered saline (PBS, pH 7.0). The mixture incubated for 1 hour at room temperature, after which it was washed 6 times with fresh PBS. After the final PBS wash was removed, HFIP was added to the labeled peptide and allowed to evaporate. The resulting pellet was stored at -20°C until use. Immediately before the experiment, the pellet was warmed to room temperature and dissolved in fresh DMSO to achieve a stock solution of 1 mM Aβ. To generate oligomers, the Aβ solution was then diluted into PBS buffer to a final concentration of 10 μM. The 10 μM solution was allowed to incubate at room temperature for 0-3 hours to produce oligomers.

Cloning, Purification, and Labeling of Apolipoprotein E

In order to specifically target the fluorophore label to a –SH group in the C-terminal region of the apoE3 protein, a cysteine-free version of apoE3 was first generated by substituting the native Cys residue at position 112 with a Ser as described previously [26]. This apoE3-like (apoE3L) gene was then used as a template for introducing a cysteine substitution at position 264 by PCR mutagenesis. The gene encoding human apoE3L-W264C was then cloned, expressed, and purified [26]. Labeling of the apoE3L was accomplished by incubating the sample with 200 μM Alexa Fluor 488 C_5-maleimide for 1 hour at room temperature in the presence of 100 μM TCEP to maintain reduced disulfides. Excess dye was removed by running the sample through a Bio-Spin 6 column (Bio-Rad, Hercules, CA). The labeled apoE3L was stored at 4°C and diluted into PBS buffer (pH 7.4) to obtain the desired concentration immediately before the experiments.

Instrumentation

We conducted our experiments using a MicroTime 200 confocal fluorescence spectroscopy system (PicoQuant GmbH, Berlin) equipped with two pulsed diode lasers (470 nm and 640 nm wavelengths, ~80 ps pulse width) operating at a repetition rate of 20 MHz. The 640 nm laser pulse was delayed by 25 ns with respect to the 470 nm laser to produce alternating laser excitation (Figure 1A). The lasers were coupled into a polarization-preserving single mode optical fiber, recollimated and then focused to a diffraction-limited spot of ~250 nm diameter by an Olympus 1.45 NA 100x oil objective to a height of 5 μm above a glass coverslip surface. The average power of each laser was 50 μW at the sample. The fluorescence emission was split by a dichroic mirror (600DCXR, Chroma Tech. Corp.), spectrally filtered with emission bandpass filters (HQ520/40 m and HQ680/75 m, Chroma Tech. Corp.), and detected by two avalanche photodiode detectors (SPCM-AQR-14, PerkinElmer). The signals were processed by a time-correlated single-photon counting board (TCSPC board, PicoHarp300,

PicoQuant), operating in time-tagged time-resolved (TTTR) mode. The TTTR mode of the data acquisition records the photon arrival time from the last excitation pulse (micro-time) with 50 ps relative time resolution, and the photon arrival time from the start of the experiment (macro-time) with 100 ns absolute time resolution. TCSPC of separate detection channels allows for the temporal analysis of all detected photons. In particular, it enables the determination of which excitation laser (470 nm or 640 nm) leads to the detection of a photon. Auto- and cross correlations were calculated and fitted using the SymPhoTime software package (PicoQuant GmbH, Berlin).

ApoE3L was labeled with a single Alexa 488 fluorophore, which exhibits an emission peak at ~519 nm after excitation with the 470 nm laser, and detected at APD 2, the "green" channel. Similarly, Aβ was labeled with a single Atto 647 fluorophore, which exhibits an emission peak at ~668 nm after excitation with the 640 nm laser, and detected by APD 1, the "red" channel. The red channel detects both free and bound Aβ and the green channel detects free and bound apoE3L. Since TCSPC electronics assigns time-tags to all detected photons, only photons that arrive at the two detectors simultaneously are analyzed. Cross correlations were formed from photons detected in the green channel while the 470 nm laser was on and from photons detected in the red channel while the 640 nm excitation laser was on. In this way, leakage of photons from Alexa 488 into the red channel and direct excitation of the Atto 647 by the 470 nm excitation laser were excluded from the analysis, eliminating sources of spurious cross correlation signals. Therefore, ALEX-FCCS allows us to resolve signals only from the truly bound species. Time traces of both Aβ and apoE3L are shown in Figure 1B.

The cross correlation signal from freely diffusing fluorescent molecules illuminated by two excitation lasers is:

$$G^{(2)}(\tau)_{XY} = \frac{\langle C_{XY}\rangle Diff_{XY}(\tau)}{V_{eff}(\langle C_X\rangle+\langle C_{XY}\rangle)(\langle C_Y\rangle+\langle C_{XY}\rangle)} \qquad (1)$$

where the term:

$$Diff_{XY}(\tau) = \left(1 + {}^{\tau}/_{\tau_{D,XY}}\right)^{-1}\left(1 + {}^{r_o^2\tau}/_{z_o^2\tau_{D,XY}}\right)^{-\frac{1}{2}}$$

denotes the temporal decay of the cross correlation function by the bound molecule with diffusion time $\tau_{D,XY}$. C_X and C_Y are the concentrations of free X and Y molecules, and C_{XY} is the concentration of bound molecules.

At lag time $\tau = 0$, equation (2) can be rewritten as [17]:

$$G_{XY}(0) = N_{XY}\left[G_x(0) * G_y(0)\right] \qquad (2)$$

G_x and G_y are the autocorrelations of channels x and y. In autocorrelation analysis, the number of molecules N in the excitation volume is inversely proportional to the amplitude of the autocorrelation function G(0), whereas in cross correlation analysis, the number of bound molecules N_{XY} is proportional to $G_{XY}(0)$ in the volume. By analyzing the auto- and cross correlation amplitudes, the number of bound molecules can be determined.

Aggregate Removal Algorithm

One problem encountered in taking accurate FCS measurements of Aβ is the presence of extremely large aggregates resulting in huge fluorescent bursts. These aggregates are most likely from Aβ that has formed large oligomers and are not necessarily a true representation of the average particle size in our sample. The large aggregates may also result from the tendency of Aβ to stick to glass surfaces, such as those used for the experimental measurements. Regardless of the cause, the large fluorescent bursts detected can skew the results of our analysis. As an example, Figure 1C shows a large Aβ aggregate with a burst size of almost ten times the average signal. To eliminate these aggregates from our data, we implemented a custom algorithm that cuts a portion of the intensity time trace when photon burst counts larger than five times the average signal are observed. The remaining portion of the time trace is then stitched back into the original time trace for photon correlation analysis.

RESULTS AND DISCUSSION

Kinetics and stoichiometry of the binding reaction- To establish the binding interactions between Aβ and apoE3L, we used a sample solution consisting of 10 μM Aβ and 10 μM apoE3L. Because micromolar Aβ in solution undergoes a process of oligomerization [27-29], a series of time measurements were performed at time zero, 15 minutes, 30 minutes, 1 hour, 3 hours, and 4 hours after introducing Aβ into solution with and without apoE3L protein. For each FCCS measurement, a small volume of this sample was diluted to less than 1 nM in PBS to ensure that the excitation volume contained at most one molecule per laser pulse, which gives a high signal to noise ratio. The data were recorded for five minutes at each time interval. To obtain an accurate statistical error distribution, the whole time series experiment was repeated five times with five independent Aβ-apoE3L samples.

The measurement taken immediately following the dilution (time zero) reveals very little correlated signal from the two probes, reflecting initially weak binding between Aβ and apoE3L. This is evident by the flat black cross correlation curve in Figure 2A. As the reaction is monitored over time, the amplitude of the cross correlation slowly increases from a value of G(0) = 0 during the initial measurement to G(0) ≈ 0.55 after 4 hours, clearly indicating binding between Aβ and apoE3L. Additional measurements were taken over a course of 48 hours, but no significant change in the correlation amplitude was observed, indicating that equilibrium was established.

Following the kinetic assessment of the binding reaction between Aβ and apoE3L over time, we determined the fraction of Aβ and apoE3L that bind to each other to form the complex. At time 4 hours, the autocorrelation was fitted to values of $G_{A\beta}(0) \approx 3.7$ and $G_{apoE3L}(0) \approx 5.2$, which are inversely proportional to the number of Aβ and apoE3L molecules in the excitation volume, or $N_{A\beta} \approx 0.27$ and $N_{apoE3L} \approx 0.19$. The cross-correlated value is $G_{A\beta/apoE3L} \approx 0.55$ (Figure 2B). Solving equation 2 with these values yields $N_{A\beta/apoE3L} \approx 0.028$, the number of fully bound particles detected in the excitation volume. This implies that approximately $N_{\%\,bound,A\beta} = \frac{N_{A\beta/apoE3L}}{N_{A\beta}+N_{A\beta/apoE3L}} \approx 9.5 \pm 3\%$ of the total Aβ concentration and $N_{N_{\%\,bound,apoE3L}} = \frac{N_{A\beta/apoE3L}}{N_{apoE3L}+N_{A\beta/apoE3L}} \approx 12.5 \pm 3\%$ of the total apoE3L concentration form a binary-complex species. It should be noted that Aβ is an inherently heterogeneous system which results in a large variance in the data.

Diffusion rate of the binary complex-
Next, we compared the diffusion time of the unbound Aβ and apoE3L to the bound species (Figure 2C) by analyzing the normalized correlation data. In principle, if every Aβ molecule binds to every apoE3L molecule, then the autocorrelation curves for the two channels would be identical. However, because the red channel measures both free and bound Aβ (Figure 2C, red) and the green channel contains data for the mixture of free and bound apoE3L (Figure 2C, green), at equilibrium we expect the two autocorrelation curves to be similar but not identical. Analysis of the autocorrelation signal at 4 hours provides average diffusion times of 110 μs for apoE3L and 100 μs for Aβ. This corresponds to a hydrodynamic radius of ~1.6 nm for both apoE3L and Aβ. By using cross correlation spectroscopy to analyze the signals from both channels arriving within a very short time interval, signals from the free proteins can be separated from that of the bound complex. The cross-correlated signal, representing a complex of Aβ-apoE3L, had a diffusion time of approximately 2 ms (Figure 2C, black) with an average hydrodynamic radius of 27 nm, which suggests that the complex in solution forms from the cooperative association of more than one apoE3L and Aβ oligomer. The formation of large, multimeric complexes of apoE and Aβ is consistent with our previous observations of apoE structure upon Aβ binding [26].

We then compared the hydrodynamic radius of the bound particle to free Aβ incubated in the absence of apoE3L (Figure 3). Aβ is known to form soluble oligomers that are conformationally and pathologically distinct [30, 31]. Under the conditions employed here, Aβ oligomers assemble into relatively disordered peptides defined as prefibrillar oligomers [31]. Monomeric Aβ has a

hydrodynamic radius of approximately 0.7 nm as measured by FCS. Rapid aggregation of 10 μM Aβ over the course of the first 2 hours resulted in many large particles approaching 100 nm hydrodynamic radius, which then dissociated afterwards to an average size of 60 nm at around 4 hours. This is consistent with previous measurements of Aβ aggregation [27, 29, 32]. Although the basis for this partial disassembly is unclear, it may be related to a reorganization of the prefibrillar oligomer, including the elimination of antiparallel interactions [33]. However, this is in contrast to the mixed reaction case, where the average bound complex particle size steadily approaches 27 nm with no observable dissociation into smaller particles. This suggests that apoE3L, when bound to Aβ, forms a more stable complex and interferes with Aβ's ability to form larger oligomers. A comparison of the hydrodynamic radii of the different particles is shown in Figure 3.

Affinity of binding-

We next investigated the binding of Aβ as a function of apoE3L concentration by FCCS. We fixed the concentration of Aβ at 10 μM while adjusting the concentration of apoE3L to 1 μM, 5 μM, 10 μM, and 20 μM. The correlation spectroscopy data were acquired 4 hours after mixing to allow for sufficient time for the mixture to reach equilibrium. The sample containing 1 μM apoE3L showed very low to no affinity for Aβ (Figure 4, inset), but the affinity increased as the concentration of apoE3L increased. Using the correlation data (following the previous section), we calculated the percentages of Aβ and apoE3L that form the bound complex. Both Aβ and apoE3L show a rapid increase in binding percentage up to 10 μM apoE3L, but appear to slow down slightly as the concentration of apoE3L approaches 20 μM. The concentration-dependence is consistent with the notion that apoE3L binding to Aβ results in a complex that involves more than one apoE molecule. We have shown that the presence of the apoE3L protein retards the progression of Aβ monomers into oligomers. Previous EPR measurements have shown that the apoE3 isoform binds Aβ with a higher affinity than does apoE4. Taken together, these results suggest that the association between the apoE4 isoform and AD outcomes may stem largely from apoE4's reduced protective ability, compared to apoE3, to form stable complexes with Aβ that facilitate Aβ clearance. Furthermore, a mechanism where apoE- Aβ complex formation proceeds via oligomeric apoE agrees with our previous EPR studies that demonstrated increased association of spin labels located on the C-terminus of apoE [26].

Conclusion-

The ε4 allele of the APOE gene represents the most significant genetic risk factor for AD [34]. The differential ability of apoE isoforms to interact and clear Aβ is likely key to the mechanism of the isoform influence on AD [26, 35]. An accumulating body of evidence demonstrates just how vital a role apoE plays in the aggregation and clearance of Aβ peptides in the brain [36, 37]. This dynamic process presents an intriguing point of intervention for rational therapies designed to prevent and/or delay the progression of AD pathology, but in order to approach this question it is first necessary to understand the precise interactions of apoE with Aβ as they relate to the deposition and clearance of Aβ peptides. Although other methods can detect both Aβ binding and oligomerization [27, 28] they are limited in their ability to describe the size and stoichiometry distribution of species in the system. We have shown using ALEX-FCCS that apoE inhibits the oligomerization of Aβ in the hydrated state. We have also demonstrated the ability of this method to report on the size and composition of biological complexes in solution, therefore providing a powerful tool for unraveling the molecular interaction of Aβ with apoE in Alzheimer's disease.

Acknowledgements

This work was performed under the auspices of the U.S. Department of Energy by Lawrence Livermore National Laboratory under Contract DE-AC52-07NA27344 and also with the support of the National Institutes of Health (R01 AG029246).

References

1. Corder, E., et al., *Gene dose of apolipoprotein E type 4 allele and the risk of Alzheimer's disease in late onset families.* Science, 1993. **261**(5123): p. 921.
2. Pericak-Vance, M., et al., *Linkage studies in familial Alzheimer disease: evidence for chromosome 19 linkage.* American Journal of Human Genetics, 1991. **48**(6): p. 1034.
3. Mahley, R.W., Y. Huang, and K.H. Weisgraber, *Detrimental Effects of Apolipoprotein E4: Potential Therapeutic Targets in Alzheimers Disease.* Current Alzheimer Research, 2007. **4**(5): p. 537-540.
4. Namba, Y., et al., *Apolipoprotein E immunoreactivity in cerebral amyloid deposits and neurofibrillary tangles in Alzheimer's disease and kuru plaque amyloid in Creutzfeldt-Jakob disease.* Brain research, 1991. **541**(1): p. 163-166.
5. Strittmatter, W.J., et al., *Apolipoprotein E: high-avidity binding to beta-amyloid and increased frequency of type 4 allele in late-onset familial Alzheimer disease.* Proceedings of the National Academy of Sciences, 1993. **90**(5): p. 1977.
6. Wisniewski, T. and B. Frangione, *Apolipoprotein E: a pathological chaperone protein in patients with cerebral and systemic amyloid.* Neuroscience letters, 1992. **135**(2): p. 235-238.
7. Holtzman, D.M., *Role of apoE/Aβ interactions in the pathogenesis of Alzheimer's disease and cerebral amyloid angiopathy.* Journal of Molecular Neuroscience, 2001. **17**(2): p. 147-155.
8. Zlokovic, B.V., et al., *Neurovascular pathways and Alzheimer amyloid beta-peptide.* Brain Pathology, 2005. **15**(1): p. 78-83.
9. Manelli, A.M., et al., *ApoE and Aβ1–42 interactions.* Journal of Molecular Neuroscience, 2004. **23**(3): p. 235-246.
10. Matthew J Sharman, M.M., Eugene Hone, Tamar Berger, Kevin Taddei, Ian J Martins, Wei Ling F Lim, Sajla Singh, Markus R Wenk, Jorge Ghiso, Joseph D Buxbaum, Sam Gandy, Ralph N Martins, *APOE genotype results in differential effects on the peripheral clearance of amyloid-beta42 in APOE knock-in and knock-out mice.* Journal of Alzheimers disease, 2010. **21**(2): p. 403-409.
11. Holtzman, D.M., et al., *Expression of human apolipoprotein E reduces amyloid-β deposition in a mouse model of Alzheimer's disease.* Journal of Clinical Investigation, 1999. **103**(6): p. R15.
12. Ehrenberg, M. and R. Rigler, *Fluorescence correlation spectroscopy applied to rotational diffusion of macromolecules.* Q Rev Biophys, 1976. **9**(1): p. 69-81.
13. Koppel, D.E., *Statistical accuracy in fluorescence correlation spectroscopy.* Physical Review A, 1974. **10**(6): p. 1938.
14. Magde, D., Elson, E. L., Webb, W. W., *Thermodynamic fluctuations in a reacting system: Measurement by fluorescence correlation spectroscopy.* Phys Rev Lett, 1972(29): p. 705-708.
15. Schwille, P., F.J. Meyer-Almes, and R. Rigler, *Dual-color fluorescence cross-correlation spectroscopy for multicomponent diffusional analysis in solution.* Biophysical journal, 1997. **72**(4): p. 1878-1886.
16. Bacia, K., S.A. Kim, and P. Schwille, *Fluorescence cross-correlation spectroscopy in living cells.* Nature methods, 2006. **3**(2): p. 83-89.
17. Kettling, U., et al., *Real-time enzyme kinetics monitored by dual-color fluorescence cross-correlation spectroscopy.* Proceedings of the National Academy of Sciences, 1998. **95**(4): p. 1416.
18. Kohl, T., et al., *A protease assay for two-photon crosscorrelation and FRET analysis based solely on fluorescent proteins.* Proceedings of the National Academy of Sciences, 2002. **99**(19): p. 12161.

19. Kim, S.A., et al., *Intracellular calmodulin availability accessed with two-photon cross-correlation.* Proceedings of the National Academy of Sciences of the United States of America, 2004. **101**(1): p. 105.
20. Kapanidis, A.N., et al., *Fluorescence-aided molecule sorting: analysis of structure and interactions by alternating-laser excitation of single molecules.* PNAS, 2004. **101**(24): p. 8936.
21. Thews, E., et al., *Cross talk free fluorescence cross correlation spectroscopy in live cells.* Biophysical journal, 2005. **89**(3): p. 2069-2076.
22. Müller, B.K., et al., *Pulsed interleaved excitation.* Biophysical journal, 2005. **89**(5): p. 3508-3522.
23. Laurence, T.A., et al., *Motion of a DNA sliding clamp observed by single molecule fluorescence spectroscopy.* Journal of Biological Chemistry, 2008. **283**(34): p. 22895.
24. Miller, A.E., et al., *Fluorescence Cross-Correlation Spectroscopy as a Universal Method for Protein Detection with Low False Positives.* Analytical chemistry, 2009. **81**(14): p. 5614-5622.
25. Blanchette CD, S.B., Fischer N, Corzett MH, Kuhn EA, Cappuccio JA, Benner WH, Coleman MA, Chromy BA, Bench G, Hoeprich PD, Sulchek TA., *Characterization and purification of polydisperse reconstituted lipoproteins and nanolipoprotein particles.* Int J Mol Sci., 2009. **10**(7): p. 2958-2971.
26. Petrlova, J., et al., *A differential association of Apolipoprotein E isoforms with the amyloid-β oligomer in solution.* Proteins, 2011. **79**(2): p. 402-16.
27. Hellstrand, E., et al., *Amyloid β-protein aggregation produces highly reproducible kinetic data and occurs by a two-phase process.* Acs Chemical Neuroscience, 2009. **1**(1): p. 13-18.
28. Petrlova, J., et al., *The Influence of Spin-Labeled Fluorene Compounds on the Assembly and Toxicity of the Aβ Peptide.* PloS one, 2012. **7**(4): p. e35443.
29. Tjernberg, L.O., et al., *Amyloid [beta]-peptide polymerization studied using fluorescence correlation spectroscopy.* Chemistry & biology, 1999. **6**(1): p. 53-62.
30. Kayed, R., et al., *Common structure of soluble amyloid oligomers implies common mechanism of pathogenesis.* Science, 2003. **300**(5618): p. 486-489.
31. Wu, J.W., et al., *Fibrillar Oligomers Nucleate the Oligomerization of Monomeric Amyloid β but Do Not Seed Fibril Formation.* Journal of Biological Chemistry, 2010. **285**(9): p. 6071.
32. Nagai, K. and H.C. Thøgersen, *Synthesis and sequence-specific proteolysis of hybrid proteins produced in Escherichia coli.* Methods in enzymology, 1987. **153**: p. 461-481.
33. Mitternacht, S., et al., *Monte Carlo Study of the Formation and Conformational Properties of Dimers of A [beta] 42 Variants.* Journal of Molecular Biology, 2011.
34. Raber, J., Y. Huang, and J.W. Ashford, *ApoE genotype accounts for the vast majority of AD risk and AD pathology.* Neurobiology of aging, 2004. **25**(5): p. 641-650.
35. Sharman, M.J., et al., *APOE genotype results in differential effects on the peripheral clearance of amyloid-β 42 in APOE knock-in and knock-out mice.* Journal of Alzheimer's Disease, 2010. **21**(2): p. 403-409.
36. Bu, G., *Apolipoprotein E and its receptors in Alzheimer's disease: pathways, pathogenesis and therapy.* Nature Reviews Neuroscience, 2009. **10**(5): p. 333-344.
37. Kim, J., J.M. Basak, and D.M. Holtzman, *The role of apolipoprotein E in Alzheimer's disease.* Neuron, 2009. **63**(3): p. 287-303.

Figure Legends

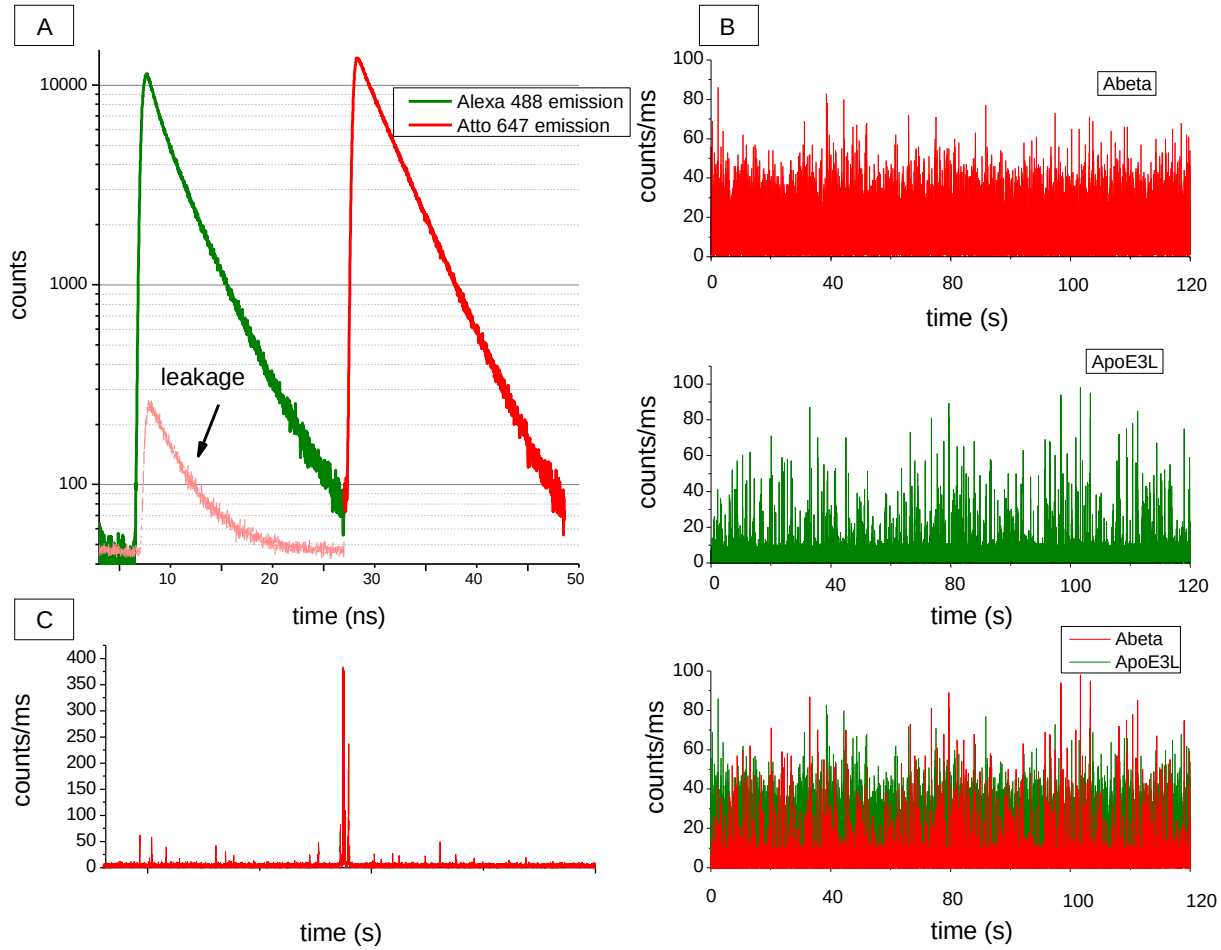

Figure 1. A) Alternating laser excitation with two pulsed diode laser sources. The 640 nm laser pulse was delayed by 25 ns with respect to the 470 nm laser to produce alternating laser excitation with a total repetition rate of 40 MHz for both lasers taken together. The emission of the red fluorophore (Atto 647) after 640 nm excitation is shown by the red decay curve, and similarly, emission of the green fluorophore (Alexa 488) after 470 nm excitation is shown by the green decay curve. Time gating (black dotted lines) allows us to remove leakage of the green fluorophore into the red channel. B) Intensity time traces recorded for two minutes produced by direct excitation of apoE3L with the 470 nm laser (top) and direct excitation of Aβ by the 640 nm laser (middle). Since all emitted fluorescence photons contain a time-tag with respect to which laser excitation produces them, only photons that overlapped in time (bottom) are used to calculate their cross correlation. C) Intensity time trace of a sample containing a large Aβ aggregate with photon burst count ten times larger than the average signal. A magnified view of the large aggregate photon burst is shown in the inset.

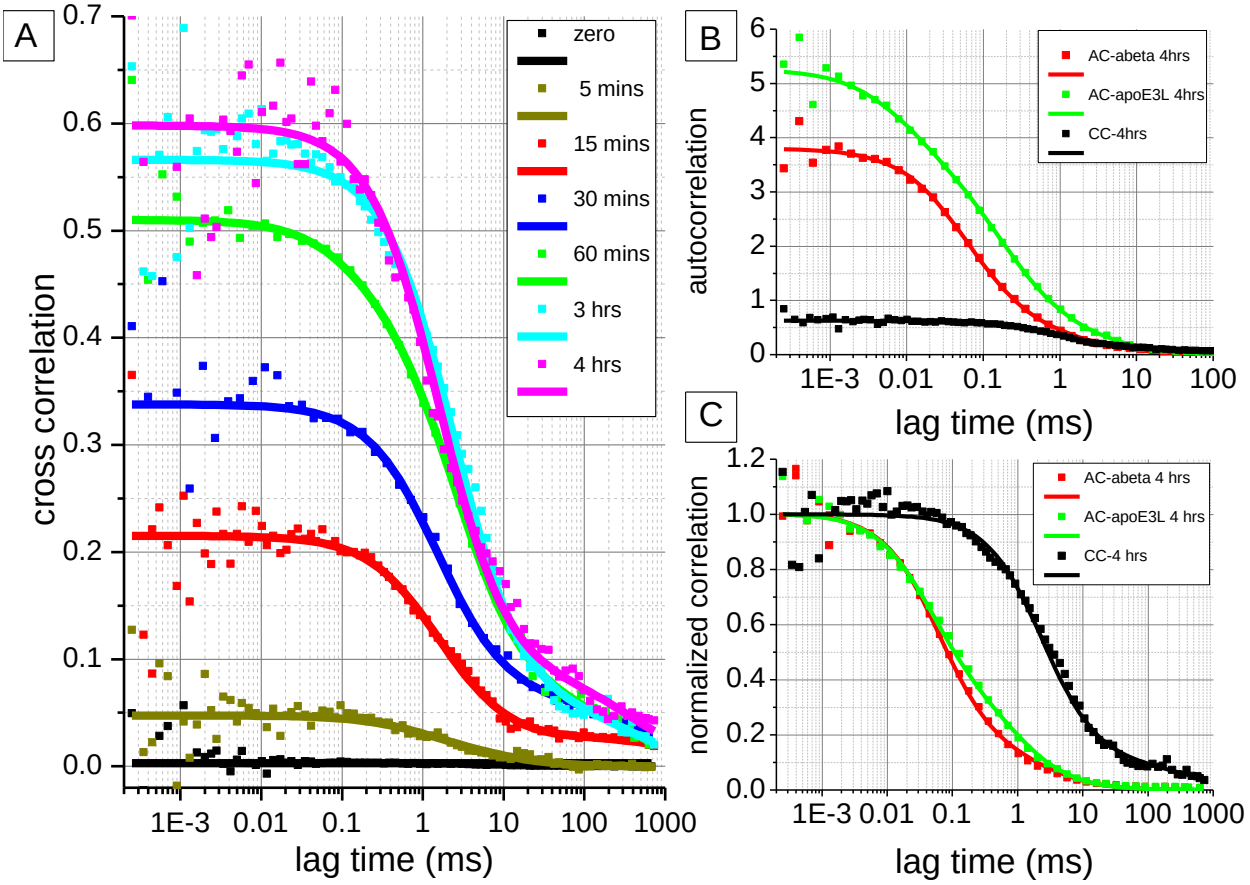

Figure 2. A) Progression of cross correlation curves for a mixture of 10 μM Aβ and 10 μM apoE3L over time. The degree of binding between the two molecules determines the amplitude of the cross correlation. The initial reaction of Aβ and apoE3L at time zero shows low correlation, indicating very weak binding. The degree of binding increases as time progresses, which is shown as a rise in the cross correlation amplitude up to time 4 hours. B) Amplitudes of the autocorrelations of the Aβ and apoE3L signals and their cross correlation at time 4 hours. C) Normalized auto and cross correlation at time 4 hours. Square dots denote raw data. Solid lines denote fitted data. (AC)-autocorrelation. (CC)-cross correlation.

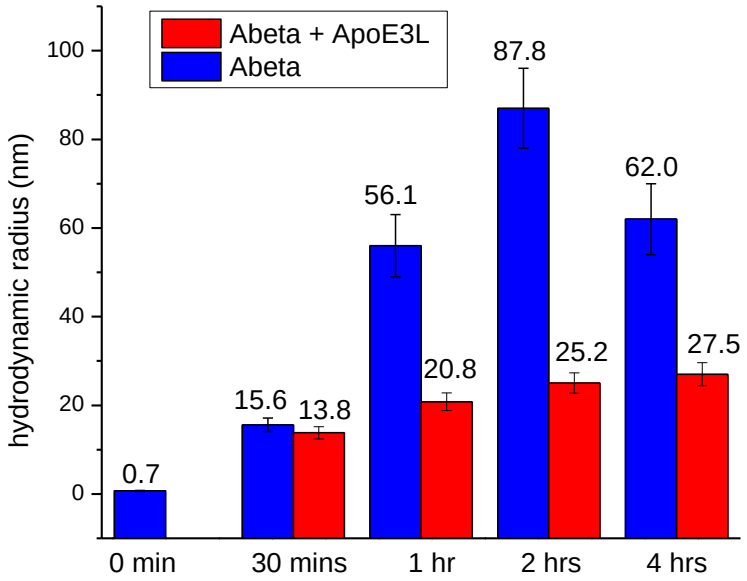

Figure 3. Bar chart of the hydrodynamic radii at different reaction times as measured by FCCS. At time 0, Aβ has a hydrodynamic radius of 0.7 nm, which increases to over 60 nm after a 4 hour reaction (blue). In the presence of apoE3L, the bound Aβ/apoE3L complex has a size of 27 nm after a 4 hour reaction. Note that at time zero, there is no binding between the two molecules and therefore the red bar has been omitted.

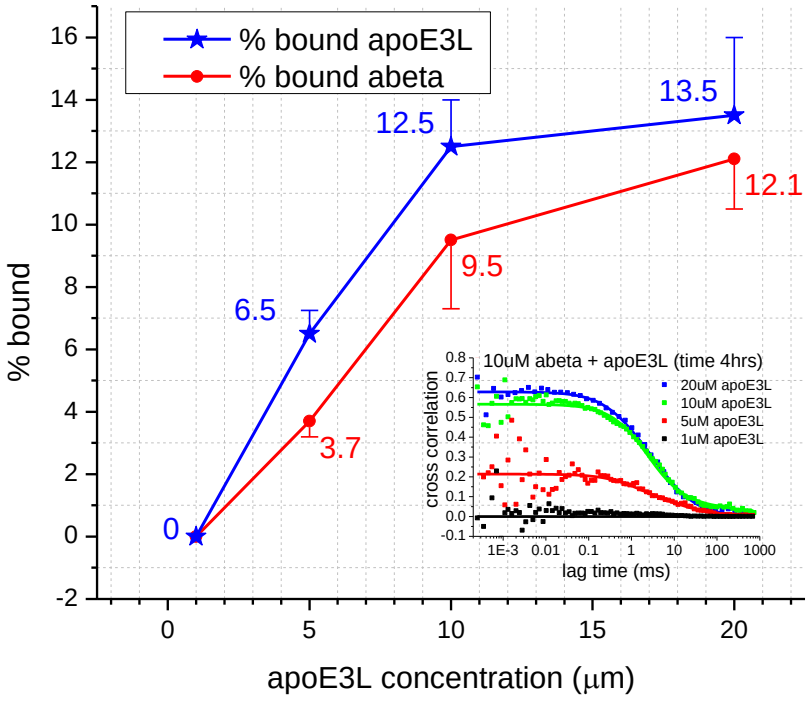

Figure 4. The fraction of bound apoE3L or Aβ in samples containing 10 μM Aβ incubated with either 1, 5, 10, or 20 μM apoE3L for 4 hours. These values were calculated from the cross correlation amplitude of 10 μM Aβ with apoE3L at 1, 5, 10, or 20 μM shown in the inset. In the presence of 1 μM apoE3L, no binding between apoE3L and Aβ was observed, as shown by the flat cross correlation trace in black. At 10 and 20 μM, the correlation amplitude increases as a result of significant binding between the two species.